# Kinetic Mechanism of $ClONO_2$ Uptake on Polycrystalline Film of NaCl†

**V. V. Zelenov,‡ E. V. Aparina,‡ S. A. Kashtanov,‡ D. V. Shestakov,§ and Yu. M. Gershenzon*,§**

*Institute for Energy Problems of Chemical Physics, Russian Academy of Sciences, Chernogolovka 142432, Russia, and N. N. Semionov Institute of Chemical Physics, Russian Academy of Sciences, Moscow 119991, Russia*

*Received: October 31, 2005; In Final Form: March 2, 2006*

Kinetic studies and the mechanism determination of $ClONO_2$ uptake on polycrystalline NaCl were carried out using a coated-insert flow tube reactor combined with high-resolution, low-energy electron-impact mass spectrometer under the following conditions: $p = 1-2$ Torr, linear flow velocity $v = 3.5-75$ m s$^{-1}$, $T = 293$ and 387 K, $[ClONO_2] = (0.5-25) \times 10^{12}$ molecules cm$^{-3}$. The salt was deposited as a film from nonsaturated aqueous solution on the sliding rod. The temporal dependences of the uptake coefficient and the partial uptake coefficients leading to a formation of the prime $Cl_2$ and HOCl products were measured for different $ClONO_2$ concentrations. These dependences are established to be described by $\gamma = \gamma_0 \exp(-t/\tau) + \gamma_s$, $\gamma_{0,s}^{-1} = a_{0,s} + b_{0,s}[ClONO_2]$. In the framework of the proposed kinetic model, the data are explained and the main elementary kinetic parameters of the uptake are evaluated. The model is based on a combination of Langmuir adsorption, formation of surface complexes on initial active sites, $Z_{ch}$, followed by their unimolecular decomposition. Decomposition is proposed to proceed concurrently in two channels, one of which is a released surface site that conserves the properties of the initial site. In the other channel, the initial $Z_{ch}$ transforms into $Z_{ph}$ followed by steady-state uptake and reproduction of final $Z_{ph}$. The model gives an analytical expression for experimental parameters $\gamma_0$, $\gamma_s$, and $\tau$ in terms of elementary rate constants and the reactant volume concentration. The final objective of the proposed model is the extrapolation of $\gamma_0$, $\gamma_s$, and $\tau$ parameters to real tropospheric conditions.

## 1. Introduction

Heterogeneous reactions are of interest in many fields of science and industry. They are important constituents of chain reactions, catalysis, catalytic combustion, etching, ore dressing, and so on. In atmospheric chemistry, these reactions have been of particular interest since 1985, when Farman et al. revealed a significant depletion of ozone layer in the Antarctic atmosphere in spring.[1] As early as 1974, Molina and Rowland had postulated a possibility of the stratospheric ozone destruction via a chain reaction mechanism:[2]

$$Cl + O_3 \rightarrow ClO + O_2$$

$$ClO + O \rightarrow Cl + O_2$$

Precursors of the chlorine atoms were proposed to be anthropogenic emissions of chlorofluorocarbon compounds that are stable in the troposphere and photolyzed in the stratosphere.

The works of Farman[1] and Molina and Rowland[2] initiated intensive field observations of the atmospheric constitution in polar and middle latitude regions as well as numerous laboratory studies. The ozone destruction proved to proceed at relatively low altitudes in the presence of polar stratospheric clouds or in the middle latitude regions in the presence of sulfuric aerosols.

Since 1985, a range of laboratory studies on the atmospheric chemistry kinetics of low-temperature heterogeneous reactions capable of generating active chlorine in polar stratospheric clouds and on sulfuric aerosols in the Junge layer have been published.

Against this background of stratospherically focused work, the fact of natural generation of halogens in the troposphere, designated "halogen activation in the troposphere", has been studied less intensively. In 1986, Bottenheim et al.[3] as well as Oltmans and Komhyr[4] observed extensive destruction of arctic troposphere ozone almost as soon as the stratospheric ozone hole was revealed. Platt et al. made a great contribution by achieving real-time measurements of active bromine (Br, BrO) in the troposphere.[5] They observed BrO radicals not only in the troposphere in polar regions but also in boundary zone over interior continental seas such as the Dead Sea and Caspian Sea. The main precursors of halogens in the troposphere are sea-salt aerosol particles that arise because of oceanic wave action and saline land erosion.

Usually, active bromine concentration in the troposphere is higher than that of active chlorine despite the fact that the abundance of bromide ions in seawater is 600 times lower than that of the chloride ions. There are two reasons for this contradictory situation. First, atomic chlorine produced in the gas phase is much more reactive with respect to hydrocarbons (HC's), which diminishes its concentration. Second, in the absence of $NO_x$ in marine troposphere, bromine concentration rises sharply ("bromine explosion") because of two-phase branching-chain processes, which include small atmospheric constituents such as Br, $Br_2$, HOBr, and $HO_2$ as well as $Br^-$ and $H^+$ ions in the water interface:[6]

$$HOBr(aq) \xrightarrow{+H^+ + Br^-} Br_2(g) \xrightarrow{h\nu} 2Br + 2O_3 \rightarrow 2BrO \xrightarrow{+2HO_2} 2HOBr(g) \rightarrow 2HOBr(aq) \quad (I)$$

The branching rate for similar chlorine process is much

† Part of the special issue "David M. Golden Festschrift".
‡ Institute for Energy Problems of Chemical Physics.
§ N. N. Semionov Institute of Chemical Physics.

10.1021/jp056272b CCC: $33.50 
Published on Web 04/04/2006

lower because the reaction[7]

$$HOCl + H^+ + Cl^- \rightarrow H_2O + Cl_2, \qquad k = 2.1 \times 10^4 \text{ mole}^{-2}\text{ s}^{-1}$$

is $10^6$ times slower compared to[8]

$$HOBr + H^+ + Br^- \rightarrow H_2O + Br_2, \qquad k = 2.3 \times 10^{10} \text{ mole}^{-2}\text{ s}^{-1}$$

In addition, the termination rate of the branching chain (I) is the reaction of halogens with HC's, which is higher in the case of chlorine.

Nevertheless, Spicer et al.[9] observed an abnormally high chlorine concentration, $[Cl_2] > 10^9$ particles $cm^{-3}$, in the littoral zone of Long Island near New York city, which is 25 times higher than that of bromine measured under the same conditions.[10] There is other evidence of abundant chlorine in the troposphere, for example, observation of morning HC's consumption,[11] that cannot be explained by the reactions of the bromine-containing compounds because of their low reactivity. This conclusion is confirmed by direct measurement of $Cl_2$ + HOCl concentration varying in the range from 26 to 254 pptv.[12] These observations have stimulated a search for mechanisms that could be responsible for the tropospheric active chlorine formation.

According to our concept, chlorine activation may be the dominant halogen activation process in the MBL near industrial regions where $NO_x$ concentration in the troposphere is high enough, whereas the active bromine plays an important role in remote locations. A simple two-phase branching-chain process is shown below, which provides active chlorine production in the MBL polluted with $NO_x$.[13−15] Here, the heterogeneous reaction of $ClONO_2$ with NaCl plays a key role:

$$ClONO_2 \xrightarrow{NaCl} Cl_2 \xrightarrow{h\nu} 2Cl \xrightarrow{2O_3} 2ClO \xrightarrow{2NO_2} 2ClONO_2 \ldots \quad \text{(II)}$$

A number of authors have investigated the reaction of $ClONO_2$ with solid NaCl.[16−22] On the basis of the large dipole moment of $ClONO_2$ molecule, the reaction has been proposed to proceed via surface intermediate complex of two dipole particles:[16]

$$ClONO_2 + NaCl \rightarrow Cl^- \cdots Na^+$$
$$\vdots \quad \vdots$$
$$Cl^+ \cdots ONO_2^- \rightarrow Cl_2 + NaNO_3, \qquad \Delta H_0^{298} = -83 \text{ kJ mole}^{-1} \quad \text{(III)}$$

Product $Cl_2$ molecules were confirmed to be the main product of the reaction.[17−22] At the same time, there is a considerable difference in the $ClONO_2$ uptake coefficients measured by previous authors. The first quantitative measurement of $ClONO_2$ uptake on NaCl was performed by Timonen et al.,[17] using a flow reactor coupled to a quadrupole mass spectrometer at 296 K and $[ClONO_2] = 3 \times 10^8 - 3 \times 10^{11}$ molecules $cm^{-3}$. The reactive uptake coefficient, $\gamma$, was determined by monitoring both $ClONO_2$ consumption and $Cl_2$ formation. For dry solid NaCl, $\gamma$ was determined to be $(4.6 \pm 3.0) \times 10^{-3}$ at $T = 296$ K. Additionally, a trace of HOCl was detected as a byproduct, which could be formed by the reaction

$$ClONO_2 + (H_2O)_{ad} \rightarrow HOCl + (HNO_3)_{ad} \qquad \text{(IV)}$$

Caloz et al. investigated the same reaction, using a Teflon-coated Knudsen reactor coupled to a quadrupole mass spectrometer.[18] Uptake of $ClONO_2$ was measured on powder, salt grains, single-crystal surfaces, and thin deposited salt layers. They measured $\gamma = 0.23 \pm 0.06$, which was independent of both $[ClONO_2]$ ($10^{10} - 10^{13}$ molecules $cm^{-3}$) and the salt substrate type. The only gas-phase product observed was $Cl_2$ molecules. The Knudsen reactor coupled to a quadrupole mass spectrometer was used in a number of additional studies.[19−20] On the basis of direct measurement of the surface residence time of $ClONO_2$ on NaCl, the $\gamma$ was determined to be of 0.1.[19] To reproduce $\gamma$ and to reveal a role of surface adsorbed water for $[ClONO_2] = 10^{10} - 10^{12}$ molecules $cm^{-3}$, Aguzzi and Rossi[20] obtained $\gamma = 0.1 \pm 0.05$ in agreement with previous results.[18,19] Gebel and Finlayson-Pitts[21] were the first to observe two-steps $ClONO_2$ uptake, that is, initial uptake with $\gamma_0 \cong 0.1$ followed by steady-state interaction with $\gamma_s = (6.5 \pm 3.0) \times 10^{-3}$ for $[ClONO_2] = 10^{12} - 10^{13}$ molecules $cm^{-3}$ and $T = 298$ K. Before these measurements, the NaCl powder was heated and pumped out to delete surface-adsorbed water. The initial uptake was interpreted as a diffusion of gas-phase reactant through the liquidlike layer of adsorbed water with simultaneous reaction inside the layer. Hoffman et al.[22] proposed a model for estimating available surface areas to correct experimental uptake coefficient. Application of this model to prior data[21] gave a corrected $\gamma_s = (2.4 \pm 1.2) \times 10^{-2}$.

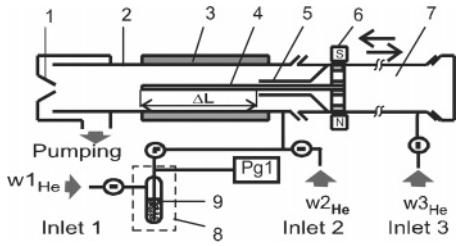


**Figure 1.** Schematic diagram of the coated-insert flow tube reactor. (1) Sampler, (2) reactor tube, (3) heating/cooling jacket, (4) sliding rod with the saline coating, (5) supporting tube, (6) leading magnet, (7) compensation volume, (8) cryostat, (9) teflon ampule with $ClONO_2$ frozen.

In the present work, the kinetics of the $ClONO_2$ consumption and the product formation is studied to determine and define the uptake coefficient in terms of rate constants for elementary steps of reactive uptake. This approach enables us to reveal the contribution of initial and steady-state steps in the total uptake, to determine a characteristic transition time between them, and, as a final objective, to extrapolate laboratory data to real tropospheric conditions.

## 2. Experimental Section

To diminish effects of coating porosity, thin films were deposited on a quartz rod from nonsaturated aqueous solutions. The roughness of the films was determined with a profilometer.

The experiments were carried out in a coated-insert flow tube reactor coupled to a phase-sensitive high-resolution low-energy electron-impact mass spectrometer.[23] Ionization near the threshold of the molecular ion formation allows the exclusion of background from dissociative ionization and identification of individual substances in a mixture of gases when their mass spectra are similar. The last consideration is especially important for the substances studied in the work.

The coated-insert flow tube reactor is shown schematically in Figure 1. Helium carrier gas flow with the addition of the $ClONO_2$ molecules moves through the outer wide glass tube (2), which is coated with a Teflon film. The thin quartz rod (4) with a saline coating can be moved along the axis of the outer tube to vary the exposure time of the salt to $ClONO_2$. The quartz rod is inserted into the reactor tube from a compensation volume

(7) through the supporting tube (5). An additional helium flow passes through the compensation volume to avoid uncontrolled salt reaction by a diffusion flux of $ClONO_2$ from the reactor (2) into the compensation volume (7). A gas sampling into the mass spectrometer is carried out through an orifice at the top of the alumina inlet cone (1). The source of $ClONO_2$ is a Teflon ampule (9) filled with Teflon capillary pieces and frozen $ClONO_2$. The ampule is placed into a homemade cryostat (8). The cryostat has a temperature range of 113−283 K with accuracy of ±0.01 K.

The $ClONO_2$ absolute concentration in the reactor is calculated from eq 1

$$[ClONO_2] = \frac{w1_{He}}{w1_{He} + w2_{He} + w3_{He}} \frac{p_{ClONO_2}(T_c)}{p_a} p n_L \quad (1)$$

where $w1_{He}$, $w2_{He}$, and $w3_{He}$ are the measured He mass flows through inlets 1, 2, and 3; $p_a$ is the absolute pressure in the ampule (9) measured by pressure gauge PG1; $p_{ClONO_2}(T_c)$ is the partial pressure of $ClONO_2$ at temperature, $T_c$, of the cryostat; $p$ is the measured pressure in the reactor; and $n_L$ is the Loschmidt number.

The mass flow of $ClONO_2$ molecules from the ampule (9) into the reactor is controlled by varying the cryostat temperature. Under conditions where the transport time of the flux $w1_{He}$ through the ampule exceeds the time of diffusion mixing considerably, $p_{ClONO_2}(T_c)$ corresponds to the saturated vapor pressure of $ClONO_2$ in the ampule. Thus, exploitation of eq 1 allows the calibration of the mass spectrometer for $ClONO_2$ and measurement at the $ClONO_2$ saturated vapor pressure as a function of temperature.

**Main Parameters of the Flow Reactor.** The inner diameter, $d_R$, of the reactor tube (2) is 1.3 cm; outer diameter, $d_r$, of the rod (4) is 0.13 cm; the maximum length of the rod, $L_r$, is 50 cm; the linear flow velocity, $v$, along the reactor is $(0.35-7.5) \times 10^3$ cm s$^{-1}$; and the characteristic pressure, $p$, is 1−2 Torr.

**Salt Sample Preparation.** Salt is deposited on the rod by dipping it into unsaturated aqueous solution of NaCl followed by drying at 200 °C. The surface covered is equal to the geometric surface of the insert rod.

**Measurement Procedure.** Ion current intensities are measured at a fixed $m/z$ without magnetic field scans using phase-sensitive ion counts. The minimum acquisition time is 2.5 s per cycle, with up to 10 cycles per experimental point. A calibration of mass spectrometer for the stable substances $NO_2$, $Cl_2$, $ClONO_2$, and HCl is obtained by introducing the measured fluxes into the reactor because the pressure in the reactor is known. Characteristic ionization energies are: $E_e = 30$ eV for $ClONO_2$ ($m/z$ 46), 11.8 eV for $NO_2$ ($m/z$ 46), 30 eV for HCl ($m/z$ 36), 30 eV for $Cl_2$ ($m/z$ 70), 30 eV for HOCl ($m/z$ 52), and 30 eV for $Cl_2O$ ($m/z$ 86). The uncertainty, $\sigma$, for every experimental intensity, $I$, measured $N$ times was calculated by

$$\sigma = \sqrt{\frac{1}{N(N-1)} \sum_{i=1}^{N} (I_i - I_{mean})^2}$$

after the acquisition procedure using soft hardware. Any intensity, $I_i$, that differs by $3\sigma$ from $I_{mean}$ was rejected. The reported experimental parameters obtained by data handling have the uncertainties consisted of two components. The fist is statistical standard error, $\sigma_{stat}$, of the measured data. The second one is determined by systematic bias, $\sigma_{sys}$, in the measured temperature, pressure, and reactant fluxes. The latter was of the order of 5%. The overall error is

$$\sigma = \sqrt{\sigma_{stat}^2 + \sigma_{sys}^2}$$

To quantitatively evaluate a validity of the model description of our experimental dependencies we have used the well-known $\chi^2$ functional

$$\chi^2 = \sum_{j=1}^{M} \left( \frac{y_j^{exp} - y_j^{model}}{\sigma_j} \right)^2 \quad (2)$$

where $y_j^{exp}$ is a value of experimental dependence $y_j^{exp}(x_j)$, $j = 1,..M$, and $y_j^{model}$ is the model approximation. At best, the value of $\chi^2$ would be of the order of $M$ that is the size of experimental array.

**Synthesis of $ClONO_2$.** Chlorine nitrate is produced by the reaction of ClF with anhydrous $HNO_3$ in stainless steel autoclave with an internal volume of 130 cm$^3$.[24] The initial reactants, ClF (0.05 M) and $HNO_3$ (0.05 M), are placed into the autoclave at −196 °C and heated slowly to 0 °C. After cooling to −78 °C, the autoclave is attached to a vacuum line allowing rapid $ClONO_2$ distillation into a reservoir held at −95 °C. The ClF reactant is produced by the reaction of $Cl_2$ with $F_2$. To prepare ClF, $F_2$ (0.1 M) and $Cl_2$ (0.1 M) are placed into the autoclave of 1000 cm$^3$ at −196 °C, heated to room temperature, and held for 4 h, followed by heating to 200 °C for 3 h. Anhydrous $HNO_3$ is produced by the reaction of $KNO_3$ with concentrated $H_2SO_4$.

The main impurity in synthesized $ClONO_2$ is $Cl_2$. To purify $ClONO_2$, the initial $ClONO_2/Cl_2$ mixture is placed in the ampule (9) at −120 °C. Upon heating to −98 °C, the ampule is pumped through the reactor while monitoring the intensity on $m/z$ 70 until $Cl_2$ vanishes from the ampule.

Possible contribution of $NO_2$ to $ClONO_2$ mass-spectral intensity is taken into account. The corrected intensity $\Delta I_{46}(30$ eV) of $ClONO_2$ is determined by the difference between a full ion current $I_{46}(30$ eV) and the contribution $I_{46}(11.8$ eV) due to $NO_2$, multiplied by relative sensitivity $\eta_{NO_2}$ of mass spectrometer to $NO_2$ at the two ionization energies:

$$\Delta I_{46}(30 \text{ eV}) = I_{46}(30 \text{ eV}) - I_{46}(11.8 \text{ eV}) \eta_{NO_2}; \quad \eta_{NO_2} = 14.85$$

**Data Treatment.** As was shown earlier,[25,26] the kinetics of consumption of a gas-phase reactant on the insert rod is described by first-order eq 3

$$-dn/dt_k = kn \quad (3)$$

where $n$ is a concentration of the gas-phase $ClONO_2$ reactant; $t_k = [0, \Delta L/v]$ is a contact time of $ClONO_2$ with the rod inserted into the reactor for the length $\Delta L$; and $v$ is a mean linear velocity of He carrier gas. The rate constant $k$ for heterogeneous uptake is shown to be expressed in terms of its kinetic ($k^k$) and diffusion ($k^d$) limits[27]

$$\frac{1}{k} = \frac{1}{k^k} + \frac{1}{k^d}$$

where[25,26]

$$k^k = \frac{\gamma c}{d_R} \frac{\rho}{1-\rho^2} \quad k^d = 4K(\rho) \frac{D}{d_R^2} \quad (4)$$

Here, $\rho = d_r/d_R$; $K(\rho = 0.1) = 1.3$ is a dimensionless diffusion rate constant;[25] $c = 2.52 \times 10^4$ cm s$^{-1}$ is a mean molecular velocity of $ClONO_2$ at 293 K; and $D$ is a diffusion coefficient

of $ClONO_2$ in He. In our case $k^d \gg k^k$; therefore, $k \cong k^k$. On the basis of eqs 3 and 4, the dependence of $\gamma$ on exposure time, $t$, of the saline covering to $ClONO_2$ flux is given by

$$\gamma(t) = \frac{\ln(I^0_{ClONO_2}/I_{ClONO_2}(t))}{t_k} \frac{d_R}{c} \frac{1-\rho^2}{\rho} \quad (5)$$

where $I^0_{ClONO_2}$ and $I_{ClONO_2}(t)$ are the intensities of $ClONO_2$ measured without a rod and with an inserted rod, respectively.

The partial uptake coefficient, $\gamma_{P1}$, describes the $ClONO_2$ uptake leading to a formation of some gas-phase product P1. The analytic expression for $\gamma_{P1}$ follows from the hypothetic kinetic mechanism

$$ClONO_2 \xrightarrow{k(t)} \text{products}$$

$$ClONO_2 \xrightarrow{k_1(t)} P_1$$

The mechanism is described by eqs 6a and b

$$-\frac{\partial[ClONO_2(t_k,t)]}{\partial t_k} = k(t)\,[ClONO_2(t_k,t)] \quad (6a)$$

$$\frac{\partial[P_1(t_k,t)]}{\partial t_k} = k_1(t)\,[ClONO_2(t_k,t)] \quad (6b)$$

where $\gamma_{P1} = \gamma \cdot k_1/k$ is proposed by definition.

On the basis of eqs 6a and b, the concentration of the product P1 can be determined at two positions of the rod: (i) the rod is inserted for the length $\Delta L$, and the signal of product P1 is recorded after some time, the uptake being steady-state and characterized by $k(t \to \infty)$, $k_1(t \to \infty)$; (ii) the rod is further inserted for the length $\Delta L$, and the signal of product P1 is recorded after insertion at once, the values of $k(t)$ and $k_1(t)$ being time-dependent

$$\frac{[P_1(\Delta L/v, t \to \infty)]}{[ClONO_2]_0} = a\,\beta_{P1}(t \to \infty)\,(1 - \exp\{-k(t \to \infty)\,\Delta L/v\}) \quad (7a)$$

$$\frac{[P_1(2\Delta L/v, t)]}{[ClONO_2]_0} = a\,\beta_{P1}(t)\,(1 - \exp\{-k(t)\,\Delta L/v\}) + a\,\beta_{P1}(t \to \infty)\exp\{-k(t)\,\Delta L/v\}\,(1 - \exp\{-k(t \to \infty)\,\Delta L/v\}) \quad (7b)$$

where $a$ is a number of molecules of the product P1 formed from one $ClONO_2$ molecule; $\beta_{P1}(t) = k_1(t)/k(t)$.

The expression for $\gamma_{P1}(t)$ follows from the ratio of 7b to 7a

$$\frac{\gamma_{P1}(t)}{\gamma_{P1}(t \to \infty)} = \frac{\gamma(t)}{\gamma(t \to \infty)} \left( \frac{[P_1(2\Delta L/v, t)]}{[P_1(\Delta L/v, t \to \infty)]} - \exp\{-k(t)\,\Delta L/v\} \right) \frac{1 - \exp\{-k(t \to \infty)\,\Delta L/v\}}{1 - \exp\{-k(t)\,\Delta L/v\}} \quad (8)$$

Here, $\gamma(t)$ and $\gamma(t \to \infty)$ are determined from consumption of $ClONO_2$. The value $\gamma_{P1}(t \to \infty)$ is calculated from eq 7a at the detection of the product $P_1(\Delta L/v,\ t \to \infty)$ from steady-state uptake $ClONO_2$ on the first part of the rod.

### 3. Experimental Results

**$ClONO_2$ Saturated Vapor Pressure Measurements.** For kinetic studies, we needed characteristic $ClONO_2$ fluxes, which correspond to saturated vapor pressure at the vapor/solid equilibrium. The temperature dependence of the saturated vapor pressure was measured using a linear relationship between pressure $p_{ClONO_2}$ and concentration $[ClONO_2]$ according to eq 1. The relative saturated vapor pressure is determined by well-known eq 9

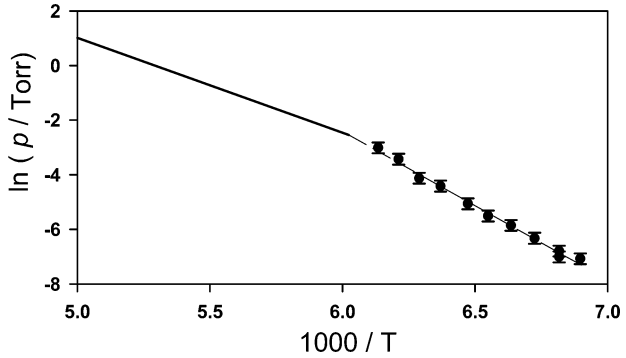


**Figure 2.** Temperature dependence of the saturated vapor pressure for $ClONO_2$. The symbols are experimental data. Dotted line shows linear regression by formula $\ln(p,\text{Torr}) = 30.254 - (5444 \pm 150)/T$. Bold solid line is taken from ref 28 data expressed by $\ln(p,\text{Torr}) = 18.396 - 3475.5/T$ for gas/liquid equilibrium.

$$\ln(p/p_0) = A - \Delta_S H°(ClONO_2)/RT \quad (9)$$

where $\Delta_S H°(ClONO_2)$ is the enthalpy of sublimation, $A$ is a calibration constant, and $p_0$ is a reference pressure.

A conversion of the relative dependence (eq 9) to the absolute one uses reference data,[28] where the temperature dependence of saturated vapor pressure is given in the range of 193−299 K for the vapor/liquid equilibrium. Additionally, a melting point, $T_m = 166$ K, was determined. The reference data[28] are shown in Figure 2 by a bold solid line. The intercept of reference and our data at the point of the phase change at $T = 166$ K enabled us to convert the relative dependence into the absolute values. The slope of our data in Figure 2 gives the enthalpy of sublimation, $\Delta_S H°(ClONO_2) = 45.26 \pm 1.25$ kJ mole$^{-1}$. The difference between the literature enthalpy of evaporation $\Delta_v H°(ClONO_2)$[28] and our $\Delta_S H°(ClONO_2)$ determines the enthalpy of melting $\Delta_m H°(ClONO_2) = 16.36 \pm 1.35$ kJ mole$^{-1}$. The absolute dependence at the vapor/solid equilibrium is given by

$$\ln p(\text{Torr}) = 30.254 - (5444 \pm 150)/T, \quad 133 < T < 163 \text{ K}$$

**$Cl_2O$ Impurity in the $ClONO_2$ Flux.** The $Cl_2O$ impurity in the $ClONO_2$ flux was detected on $m/z$ 86 at $E_e = 30$ eV. Figure 3 shows temporal dependences of $ClONO_2$ and $Cl_2O$ concentrations after an initial flux of $ClONO_2$ into the reactor. The sum of their concentrations is seen to be constant over all times of observation. This means that $Cl_2O$ impurity is a product of partial decomposition of $ClONO_2$ in the delivery line. After passivating the delivery line by $ClONO_2$ flow for 3 h, the content of $Cl_2O$ in $ClONO_2$ becomes less than 5%. Nevertheless, to correct the variation in the $ClONO_2$ concentration during the experiment, the contribution of $[Cl_2O]$ was taken into account. Calibration of the mass spectrometer for $Cl_2O$ was carried out using the product balance $[ClONO_2(t=0)] = [ClONO_2(t)] + 2[Cl_2O(t)]$, as well as a relationship between $ClONO_2$ and $Cl_2O$ concentrations and their mass-spectral intensities $I_{86} = [Cl_2O] \cdot \eta(Cl_2O)$, $\Delta I_{46} = [ClONO_2] \cdot \eta(ClONO_2)$. A relative sensitivity $\eta(ClONO_2)/\eta(Cl_2O) = 0.14$ for the mass spectrometer was determined, taking into account all continuum of experimental points $I_{86}(t_i)$, $\Delta I_{46}(t_i)$ and the analytic relations given above. The relative sensitivity obtained enables us to convert the intensity

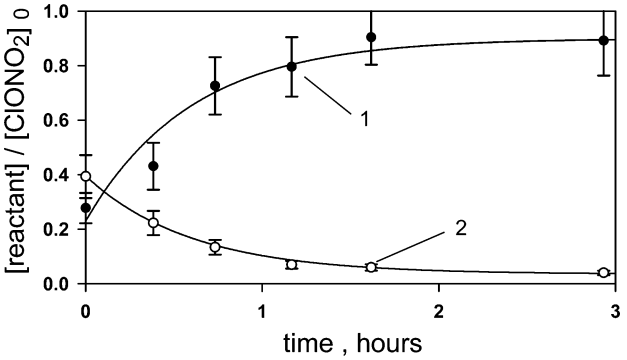


**Figure 3.** Temporal variation in the initial mixture of the reactants at $ClONO_2$ flux from the ampule of $1 \times 10^{15}$ molecules $s^{-1}$. The concentration $[ClONO_2]_0 = 5.5 \times 10^{12}$ molecules $cm^{-3}$ is calculated by eq 1. (1), experimental $[ClONO_2(t)]/[ClONO_2]_0$; (2), experimental $[Cl_2O(t)]/[ClONO_2]_0$. Solid curves show their approximations by $0.23 + 0.67(1 - \exp(-t/\tau))$ and $0.035 + 0.36\exp(-t/\tau)$, respectively, with $\tau = 36$ min.

ratio $I_{86}/I_{46}$ into the $[Cl_2O]/[ClONO_2]$ ratio. Figure 3 shows recalculated data. The corrected $ClONO_2$ concentration in the reactor was calculated by the formula

$$[ClONO_2] = \frac{[ClONO_2]_0}{1 + \frac{2I_{86}}{\Delta I_{46}} \frac{\eta(ClONO_2)}{\eta(Cl_2O)}}$$

where $[ClONO_2]_0$ is the $ClONO_2$ concentration determined by eq 1.

An estimated upper limit value of the $Cl_2O$ uptake coefficient on NaCl was obtained from measurement of the $Cl_2O$ intensities at two positions of the rod, that is, $I_{86}(L = 0) = 566 \pm 10$ Hz and $I_{86}(L = 10\text{ cm}) = 576 \pm 11$ Hz under the following experimental conditions: $T = 293$ K, $p = 2.02$ Torr, $v = 220$ cm $s^{-1}$, $t_k = \Delta L/v = 4.5 \times 10^{-2}$ s, $[ClONO_2]_0 = 1.9 \times 10^{12}$ molecules $cm^{-3}$, and $[Cl_2O] = 3.5 \times 10^{11}$ molecules $cm^{-3}$. Evaluated $\gamma_{Cl_2O} \leq 2.7 \times 10^{-4}$ follows from the formula

$$\gamma_{Cl_2O} \leq \frac{d_R}{(d_r/d_R)\, c_{Cl_2O}\, t_k} \sqrt{\left(\frac{\delta I_0}{I_0}\right)^2 + \left(\frac{\delta I_{10}}{I_{10}}\right)^2}$$

Thus, the upper estimation of $\gamma_{Cl_2O}$ is 1 order of magnitude less than that of $ClONO_2$ and the $Cl_2O$ impurity of 5% does not affect the results for $ClONO_2$ uptake.

**Total and Partial Uptake Coefficients for $ClONO_2$/NaCl.** Temporal consumption of the $ClONO_2$ reactant and formation of $Cl_2$ and HOCl products were investigated for $[ClONO_2] = (5 \times 10^{11} - 2.5 \times 10^{13})$ molecules $cm^{-3}$. Figure 4 shows typical temporal dependences of $ClONO_2$, $Cl_2$, and HOCl signals at initial insertion of the rod covered with NaCl into the flux of gas-phase reactant and after reinsertions of the same part of the rod. Figure 5 shows the total and partial uptake coefficients calculated from the data in Figure 4, using eqs 5 and 8. At the initial exposure, a sharp drop in the uptake coefficient is seen. Further diminishing the coefficient down to some steady-state $\gamma_s$ occurs with a time constant of the order of 10 s, the $\gamma_s$ being stable for a long time. At the beginning, HOCl is the main product of the reaction. HOCl formation is sure to result from reaction IV due to chemisorbed water on the surface of saline covering. In the course of initial reaction of fresh salt coating, the $H_2O$ molecules are consumed. Therefore, the HOCl product is not present for repetitive rod insertions. Similar temporal behavior of $\gamma(t)$ on fresh saline coverings was observed

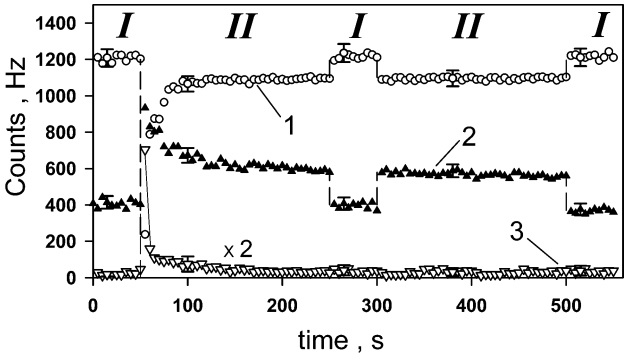


**Figure 4.** Temporal variations in the mass-spectral signals for $ClONO_2$ reactant (1) and the products $Cl_2$ (2), HOCl (3, on an enlarged scale) at two positions of the rod: (*I*), without rod and (*II*), with rod inserted. Procedure was being carried out under conditions $[ClONO_2] = 2.5 \times 10^{12}$ molecules $cm^{-3}$, $p = 2$ Torr, $T = 293$ K, $\Delta L = 10$ cm, $t_{res} = 4.9 \times 10^{-2}$ s.

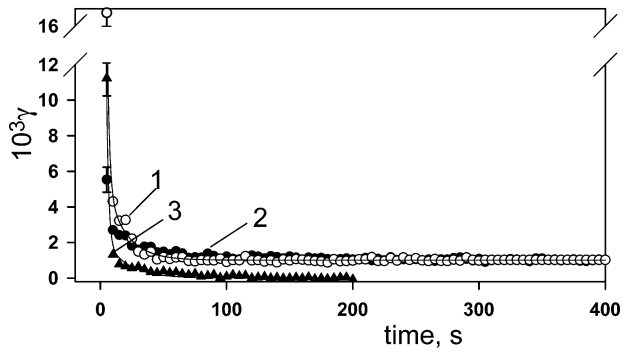


**Figure 5.** Temporal variation in the total and partial uptake coefficients for $ClONO_2$ uptake on fresh NaCl under conditions given in the capture to Figure 4. The symbols are experimental data for $ClONO_2$ consumption (1), $Cl_2$ (2) and HOCl (3) formation. Solid curves show approximation by eq 25 with parameters $\gamma_{ch}$, $\gamma_s$, $\gamma_{ini}$, $\tau_{ch}$, $\boldsymbol{\tau}_{ini}$ of $6.7 \times 10^{-3}$, $1.01 \times 10^{-3}$, 0.2, 15.3 s, 1.7 s for $ClONO_2$; of $2.6 \times 10^{-3}$, 0, 0.2, 17.7 s, 1.6 s for HOCl; of $7.1 \times 10^{-3}$, $1.01 \times 10^{-3}$, 0, 11 s, 0 s for $Cl_2$.

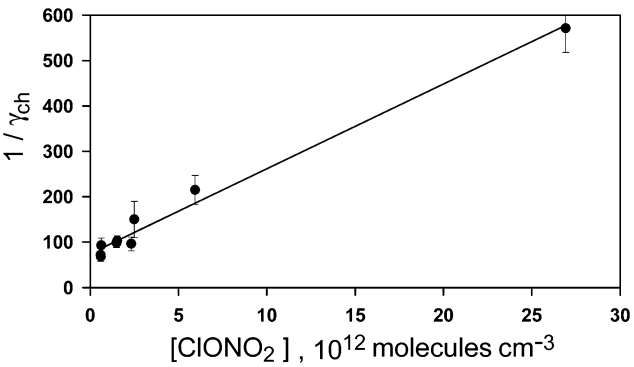


**Figure 6.** Dependence of the uptake coefficient $\gamma_{ch}$ on $ClONO_2$ concentration for the initial uptake of $ClONO_2$ on NaCl at $T = 293$ K. The symbols are experimental data. The solid line shows linear regression by $1/\gamma_{ch} = a_{ch} + b_{ch}[ClONO_2]$ at $a_{ch} = 74.7 \pm 7.7$, $b_{ch} = (18.7 \pm 0.8) \times 10^{-12}$ molecules$^{-1}$ $cm^3$.

previously for $NO_3$ uptake on NaCl and NaBr.[30−33] Figures 6−8 will be discussed in the framework of the kinetic mechanism presented in the next section.

## 4. Discussion

**Morphology of the NaCl Surface Exploited.** There are two uncertainty factors that have to be taken into account to determine trace gas uptake on saline coverings. These are the porosity and roughness of the surface. The first was analyzed

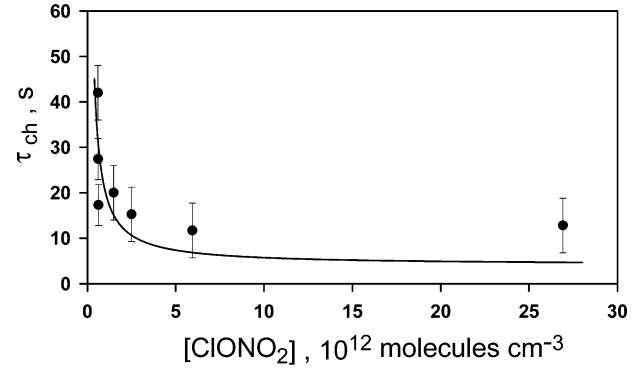


**Figure 7.** Dependence of the characteristic time $\tau_{ch}$ on $ClONO_2$ concentration for the initial uptake of $ClONO_2$ on NaCl at $T = 293$ K. The symbols are experimental data. The solid curve shows approximation by $\tau_{ch} = \tau_0(1 + n_{th}/[ClONO_2])$ at $\tau_0 = 4.1 \pm 0.6$ s, $n_{th} = 4 \times 10^{12}$ molecules $cm^{-3}$.

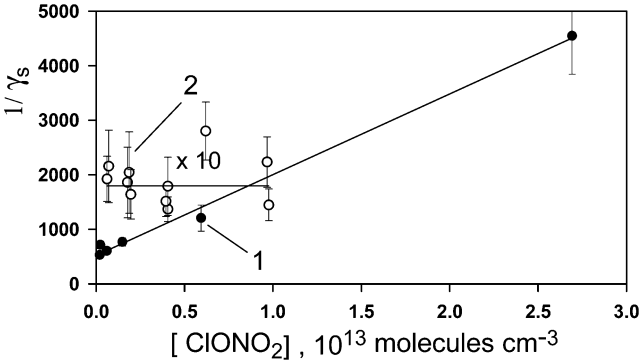


**Figure 8.** Dependence of the uptake coefficient $\gamma_s$ on $ClONO_2$ concentration for steady-state uptake of $ClONO_2$ on NaCl. The symbols are experimental data at 293 K (1) and 387 K (2, on an enlarged scale). The solid lines show linear regressions by $1/\gamma_s(293\ K) = a_s + b_s[ClONO_2]$ at $a_s = 521 \pm 61$, $b_s = (14.8 \pm 0.6) \times 10^{-11}$ molecules$^{-1}$ $cm^3$; $1/\gamma_s(387\ K) = 179.6 \pm 21.5$.

previously by Rossi.[34] In fact, porosity increases chemically active surfaces as compared to a geometric surface area because of diffusional gas penetration. This factor is most relevant in experiments on powders. The reactive surface of coarse grains is shown by electron microscopy to approach their geometric surface. Gas-phase species react on the first surface layer and do not have the opportunity to diffuse inside when $\gamma \geq 0.1$. Film coatings used in this study have the least internal surface.[34]

The second uncertainty factor is roughness of the surface. Using a profilometer with linear resolution of 50 Å, a roughness of the film coatings deposited from aqueous solutions turns out to increase the surface area no more than 15%.[35]

**Adsorption Sites of the NaCl Crystallites.** Two steps for $ClONO_2$ uptake on fresh NaCl are observed in the experiments. We associate the difference between them with the difference in the properties of the adsorption sites where the uptake occurs. According to literature data, there are three basic types of adsorption sites, each of them having its own energy distribution: (a) sites capable of chemisorption, even up to dissociative chemisorption; their initial surface density for the fresh NaCl surface is of ~1%[36] with respect to the total surface site density $Z_0 = 6.4 \times 10^{14}$ sites $cm^{-2}$;[37] (b) the defects of crystalline structure with the surface density of ~20%;[38] and (c) the vacant sites generated on conditionally defectless surface. Their action is controlled by physisorption of gas-phase reactants, the heat of adsorption being lower compared to those of a and b sites. Reactive uptake on the c sites is shown to stop at once after the first interaction between the gas-phase molecule and the site; the resulting two-dimensional surface product is not transformed into a three-dimensional crystalline structure.[39]

Uptake on the a sites results in the highest energy release. Uptake is likely to proceed without regeneration of the sites. Uptake on the b sites appeared to be similar to that on crystal defects containing chemisorbed water. Water molecules are trapped by the b sites during coating preparation and cannot be removed during surface drying because of high heat of adsorption. While participating in the reaction with $ClONO_2$, the b sites can regenerate or convert to the c sites with lower heat of adsorption, the total density of the sites being constant. Transformation of the b sites into the c sites during reactive uptake is supposed to lead to a transition between the uptake mechanisms, that is, from chemisorption at the beginning to the physisorption responsible for the steady-state process.

Reproduction of the c sites can be explained only by the presence of surface-adsorbed water. According to Seisel et al.,[40] even dry NaCl monocrystals contain adsorbed water, which corresponds to ~10−20 formal monolayers. During uptake of a $ClONO_2$ molecule on the c site, water molecules give a mobility to the $NaNO_3$ product. Surface mobility of the products enables them to be rearranged and form a new three-dimensional crystalline phase. Thus, although not converted in the reaction, the water remains and reproduces the c defects.

**Kinetic Mechanism of $ClONO_2$ Initial Uptake.** Interaction between $ClONO_2$ molecules and the NaCl surface is proposed to be described by the reaction mechanism

$$ClONO_2 + Z_{ch} \underset{k_d}{\overset{k_a}{\rightleftharpoons}} ClONO_2 \cdots Z_{ch} \begin{cases} \xrightarrow{\varphi k_r} Z_{ph} + P_1 \\ \xrightarrow{(1-\varphi)\cdot k_r} Z_{ch} + P_2 \end{cases} \qquad (V)$$

Mechanism V includes reversible chemisorption of $ClONO_2$ molecules on the $Z_{ch}$ sites followed by unimolecular decomposition of the surface complex. The decomposition proceeds via two competitive channels. One of them reproduces initial $Z_{ch}$, and another one transforms it into the $Z_{ph}$ site that has different reactive and adsorptive properties. Here, $k_a = \alpha\, c/4$ is the adsorption rate constant; $k_d = A_d \exp(-Q/RT)$ is the desorption rate constant; $\alpha$ is a sticking coefficient; $c$ is the mean molecular velocity of $ClONO_2$; $A_d \cong 10^{13}$ $s^{-1}$ is the preexponential factor; $k_r$ is the rate constant of unimolecular decomposition of the surface complex $ClONO_2 \cdots Z_{ch}$; and $\varphi$ is a probability to transform site $Z_{ch}$ into site $Z_{ph}$ in the course of unimolecular decomposition.

According to this scheme, the decomposition with the rate constant $\varphi k_r$ transforms initial active sites $Z_{ch}$ into sites $Z_{ph}$ responsible for steady-state uptake. The latter reproduces itself and the surface density of $Z_{ph}$ stays unaltered. The decomposition with the rate constant $(1-\varphi)k_r$ reproduces initial $Z_{ch}$ and gives some product P2. The contribution of $Z_{ch}$ sites in a total surface density of active sites diminishes because a part of them transforms into $Z_{ph}$.

A prerequisite for the proposed chain mechanism of the initial uptake is based on the large number of NaCl monolayers that are spent in the course of the uptake. The evaluation follows from equality of a number of spent $ClONO_2$ molecules to a number of the reacted surface sites under assumption that the uptake of one molecule leads to consumption of one surface site. This equality is expressed by eq 10

$$\frac{[ClONO_2]cS}{4} \int_0^\infty \gamma(t)\, dt = n_S S \qquad (10)$$

where $[ClONO_2]$ is the $ClONO_2$ volume concentration; $c = 2.53 \times 10^4$ cm $s^{-1}$ is a mean molecular velocity; $S$ is a geometric surface of the saline covering; $n_S$ is the surface density of reacted sites; $\gamma(t)$ is the approximation of the data in Figure 5 by function $10^3\gamma(t) = 6.67\ \exp(-t/15.25) + 200\ \exp(-t/1.757)$ without the contribution of the steady-state uptake ($\gamma_s = 1.01 \times 10^{-3}$).

A number of spent monolayers are determined by the relation $n_S/(f Z_0)$ because only $f = 0.2$ part of the total density $Z_0$ of active sites are capable of reactive uptake. The evaluation gives 56 monolayers. It means that initial uptake proceeds via a chain mechanism with partial reproduction of the initial sites.

On the basis of the reaction mechanism (V) and on the simplest Langmuir adsorption model, a variation in the total number of $ClONO_2$ molecules on the salt surface and in the gas phase is determined by eqs

$$V\frac{d}{dt}n_V = -(J_a - J_d)Sf \tag{11}$$

$$SZ_0\frac{d\theta_{ch}}{dt} = (J_a - J_d - J_r)S \tag{12}$$

$$SZ_0\frac{d\theta_{ph}}{dt} = \varphi J_r S \tag{13}$$

where $n_V$ is the $ClONO_2$ concentration in the gas phase; $\theta_{ch} \times Z_0$ and $\theta_{ph} \times Z_0$ are surface density of $Z_{ch}$ and $Z_{ph}$ sites; $S$ is a geometric surface of the rod covered with NaCl and introduced for the length $L$ into the $ClONO_2$ flux; $V$ is a reactor volume corresponding to the length $L$; $f = 0.2$ is a fraction of $Z_0$ capable of reactive uptake;[38] $J_a$, $J_d$, and $J_r$ are the mass fluxes of $ClONO_2$ onto unit surface corresponding to adsorption, desorption, and reaction, respectively

$$J_a = k_a n_V(1 - \theta_{ch} - \theta_{ph}), \quad J_d = k_d\theta_{ch}Z_0, \quad J_r = k_r\theta_{ch}Z_0 \tag{14}$$

On the assumption of dynamic equilibrium between the fluxes, that is, for

$$J_a - J_d - J_r \cong 0 \tag{15}$$

a relation (eq 16) between $\theta_{ch}$ and $\theta_{ph}$ follows from eq 15

$$\theta_{ch} = \frac{1 - \theta_{ph}}{1 + (n_{th}/n_V)} \tag{16}$$

where $n_{th} = (k_d + k_r)(Z_0^{NaCl}/k_a)$ is some threshold volume concentration of $ClONO_2$, which corresponds to unimolecular covering in Langmuir model.

Taking into account initial condition $\theta_{ph}(t = 0) = 0$, after substitution of $\theta_{ch}$ from eq 16 into eq 13, we find an explicit form for $\theta_{ph}$

$$1 - \theta_{ph} = \exp\left(-\frac{\varphi k_r t}{1 + (n_{th}/n_V)}\right) \tag{17}$$

On the basis of eq 16, expression for $\theta_{ch}$ is given by

$$\theta_{ch} = \frac{1}{1 + (n_{th}/n_V)}\exp\left(-\frac{\varphi k_r t}{1 + (n_{th}/n_V)}\right) \tag{18}$$

On the basis of definition 14 and assumption 15, eq 11 now transforms into

$$V\frac{d}{dt}n_V = -\frac{k_r Z_0 Sf}{1 + (n_{th}/n_V)}\exp\left(-\frac{\varphi k_r t}{1 + (n_{th}/n_V)}\right) \tag{19}$$

Alternatively, a formal definition of $\gamma$ is given by

$$V\frac{d}{dt}n_V = -\frac{\gamma c}{4}n_V S \tag{20}$$

Comparison of eqs 19 and 20 gives explicit expression for $\gamma$

$$\gamma = \frac{4Z_0 f}{c}\frac{k_r}{n_V + n_{th}}\exp\left(-\frac{\varphi k_r t}{1 + (n_{th}/n_V)}\right) = \gamma_{ch}\exp\left(-\frac{t}{\tau_{ch}}\right) \tag{21}$$

where

$$\gamma_{ch}^{-1} = a_{ch} + b_{ch}n_V, \quad \tau_{ch} = \frac{1}{\varphi k_r}\left(1 + \frac{n_{th}}{n_V}\right) \tag{22,23}$$

with

$$a_{ch} = \frac{1}{\alpha f}\left(1 + \frac{k_d}{k_r}\right), \quad b_{ch} = \frac{1}{f}\frac{c}{4k_r Z_0}, \quad n_{th} = \frac{a_{ch}}{b_{ch}}$$

Note that combined eqs 12 and 13 can be resolved relative to the sought quantities $\theta_{ch}(t)$ and $\theta_{ph}(t)$ without assumption (eq 15) of quasi stationarity on $\theta_{ch}$. In this case, the expression for $\gamma$ follows from the equating of right parts of eqs 11 and 20, taking into account terms $J_a$ and $J_d$ from eq 14

$$\gamma = \gamma_{ch}\exp\left(-\frac{t}{\tau_{ch}}\right)\left\{1 - \exp\left(-\frac{t}{\tau_{ini}}\right)\right\} + \gamma_{ini}\exp\left(-\frac{t}{\tau_{ini}}\right) \tag{24}$$

where

$$\gamma_{ini} = \alpha f, \quad \tau_{ini} = \frac{1}{k_d + k_r}\frac{1}{1 + (n_V/n_{th})}$$

The values of $\gamma_{ch}$ and $\tau_{ch}$ are the same as those in eq 22 under dynamic equilibrium. The time $\tau_{ini}$ characterizes a transition from empty surface to dynamic equilibrium between the adsorption, desorption, and reaction fluxes. In one of the extreme cases, that is, at $n_V \ll n_{th}$, this time is determined by the desorption rate and approximately equals a residence time $k_d^{-1}$ for adsorbed molecule on the surface. In the other extreme case, that is, at unimolecular covering, the time $\tau_{ini}$ is determined by the adsorption rate and equals $4Z_0/(cn_V)$.

Equations 21 and 24 for $\gamma$ describe the initial uptake on the $Z_{ch}$ sites only. In fact, in the course of the initial uptake the $Z_{ph}$ sites interact with $ClONO_2$ as well. Formally, it means that $J_r$ from eq 14 must contain an additional term $k_{r\,2}\theta_{ph}Z_0$. Here $k_{r\,2}$ is the rate constant of unimolecular decomposition of the surface complexes $ClONO_2\cdots Z_{ph}$. Substitution of $J_{r\,2} = k_{r2}\theta_{ph}Z_0$ into eq 19 gives additional contribution in $\gamma$, that is, $\gamma_s(1 - \exp(-t/\tau_{ch}))$, where $\gamma_s$ is the uptake coefficient of the steady-state uptake that occurs on the $Z_{ph}$ sites only. Thus, in summary, an uptake coefficient that describes both initial and steady-state uptake is presented by formula

$$\gamma = \gamma_{ch}\exp(-t/\tau_{ch})\{1 - \exp(-t/\tau_{ini})\} + \gamma_s(1 - \exp(-t/\tau_{ch})) + \gamma_{ini}\exp(-t/\tau_{ini}) \tag{25}$$

**Elementary Kinetic Parameters of the Initial Uptake.** Figures 6 and 7 show summarized data on dependences of $\gamma_{ch}$

**TABLE 1: Summarized Elementary Constants for Reactive $ClONO_2$ Uptake on Polycrystalline Film of NaCl at 293 K**

| stage | $n_{th}$, $10^{12}$cm$^{-3}$ | $k_d$, s$^{-1}$ | $k_r$, s$^{-1}$ | $1/\varphi$ |
|---|---|---|---|---|
| initial | $4.0 \pm 0.4$ | $37 \pm 4$ | $2.6 \pm 0.1$ | $11 \pm 1.6$ |
| steady-state | $3.5 \pm 0.4$ | $34.7 \pm 4.3$ | $0.3 \pm 0.2$ | |

and $\tau_{ch}$ on the $ClONO_2$ volume concentration. The data were obtained by handling the temporal dependences similar to the ones shown in Figure 5. The treatment was produced by eq 25. The last of the terms in eq 25 is responsible for a nonstationary uptake and gives an essential contribution in only several first points of the experimental $\gamma(t)$. Besides, an uncertainty in the start of measurement is of 1 s. Therefore, precision of the $\tau_{ini}$ determination is low. To exclude effect of this stage of the uptake, several first points of experimental $\gamma(t)$ were not taken into account at the first step of the treatment. All assemblage of the residuary experimental points are described now by the simplified expression

$$\gamma(t) = \gamma_{ch} \exp(-t/\tau_{ch}) + \gamma_s(1 - \exp(-t/\tau_{ch})) \quad (26)$$

Parameters $\gamma_{ch}$ and $\tau_{ch}$ were obtained by fitting of the experimental $\gamma(t)$ with eq 26, $\gamma_s$ being taken independently from the stationary part of the experimental $\gamma(t)$. After that, all of the experimental points, including the first ones deleted earlier, were approximated by eq 25, where the sole sought value was $\tau_{ini}$. The value of $\gamma_{ini}$ was taken as 0.2 based on its expression in terms of parameters $\alpha$ and $f$ given in eq 24. Note that our model predicts a sharp initial drop in $\gamma(t)$, which is likely explained by the initial nonstationary uptake.

Elementary parameters were determined from approximation of the dependences in Figures 6 and 7 by analytical expressions 22 and 23. The parameters $a_{ch} = 74.7 \pm 7.7(1\sigma)$ and $b_{ch} = (18.68 \pm 0.8(1\sigma)) \times 10^{-12}$ molecules$^{-1}$cm$^3$ were obtained from linear regression of data in Figure 6 by eq 22. Here, $\sigma$ is one standard error. Note that $\chi^2 = 8$ calculated by eq 2 is in good agreement with the number of experimental points in Figure 6. On the basis of eq 22, the expression of parameters $a_{ch}$ and $b_{ch}$ in terms of rate constants $k_d$ and $k_r$ gives $k_r = 2.6 \pm 0.1$ s$^{-1}$ and $k_d = 37 \pm 4$ s$^{-1}$. The ratio $a_{ch}/b_{ch}$ gives the threshold volume concentration $n_{th} = (4.0 \pm 0.4) \times 10^{12}$ molecules cm$^{-3}$. For calculation, the following parameters were used: $\alpha = 1$, $f = 0.2$,[38] $c = 2.53 \times 10^4$ cm s$^{-1}$, $Z_0^{NaCl} = 6.4 \times 10^{14}$ sites cm$^{-2}$.

On the basis of eq 23, the data in Figure 7 were approximated by function $\tau_{ch} = \tau_0(1 + n_{th}/[ClONO_2])$ where the sole sought parameter was $\tau_0$, the threshold concentration $n_{th}$ being taken from the data in Figure 6. The result of this approximation is $\tau_0 = 4.1 \pm 0.6(1\sigma)$ s with $\chi^2 = 16$ for size = 7. On the basis of its definition, $\tau_0 = 1/\varphi\, k_r$, and the calculated $k_r$, the parameter $1/\varphi$ is found to be $11 \pm 1.6$ s. The parameter $\varphi$ represents the probability of transforming site $Z_{ch}$ into site $Z_{ch}$ during unimolecular decomposition of the surface complex $ClONO_2 \cdots Z_{ch}$. The reciprocal value $1/\varphi$ characterizes the number of catalytic cycles of the reaction before transformation of $Z_{ch}$ into $Z_{ph}$.

**Steady-State $ClONO_2$/NaCl Uptake.** Figure 8 shows dependences of the uptake coefficient on the $ClONO_2$ volumetric concentration for steady-state uptake at two temperatures, 293 and 387 K. The regression form is likely to be valid because $\chi^2$ corresponds exactly to the number of the experimental points for both temperatures. The dependences agree well with the model proposed by us earlier for the $NO_3$/NaCl and $NO_3$/NaBr systems.[30−33] The steady-state uptake can be described by the scheme

$$ClONO_2 + Z_{ph} \underset{k_d}{\overset{k_a}{\rightleftharpoons}} ClONO_2 \cdots Z_{ph} \xrightarrow{k_r} Z_{ph} + \text{products} \quad \text{(VI)}$$

On the basis of the proposed mechanism and precisely described in the previous section, the uptake coefficient is expressed by

$$\gamma_s^{-1} = \frac{1}{\alpha f_{ph}} \frac{k_d + k_r}{k_r} \left(1 + \frac{n_V}{n_{th}}\right) \quad (27)$$

where $f_{ph}$ is a relative portion of the $Z_{ph}$ surface sites in the total surface density $Z_0^{NaCl}$; and $n_{th} = Z_0^{NaCl}(k_d + k_r)/k_a$. Generally, the values of $k_r$, $k_d$, and $n_{th}$ differ from those for the initial uptake. Similar to the initial uptake case, we can

**TABLE 2: Comparison with Literature Data**

| type of uptake coefficient | value | substrate type | $T$, K | ref | comments |
|---|---|---|---|---|---|
| $\gamma_s$ | $(4.6 \pm 3.1) \times 10^{-3}$ | granules | 296 | 17 | independent of $[ClONO_2] = (3-3000) \times 10^8$ molecules cm$^{-3}$ |
| $\gamma_0$, $\gamma_s$ | $(2.3 \pm 0.6) \times 10^{-1}$ | solid powder, grains, crystals, thin films of crystallites | 298 | 18 | $\gamma_0 \approx \gamma_s$, independent of both substrate type and $[ClONO_2] = 10^{10}-10^{13}$ molecules cm$^{-3}$ |
| $\gamma_0$ | 0.1 | polycrystalline film | 298 | 19 | |
| $\gamma_0$, $\gamma_s$ | $0.1 \pm 0.05$ | solid NaCl | 298 | 20 | |
| $\gamma_0$ | $\geq 0.1$ | solid NaCl | 298 | 21 | |
| $\gamma_s$ | $(6.5 \pm 3.0) \times 10^{-3}$ | | | | |
| $\gamma_0$ | $0.42 \pm 0.46$ | synthetic | 298 | 21 | |
| $\gamma_s$ | $0.16 \pm 0.2$ | sea salt | | | |
| $\gamma_0$, $\gamma_s$ | $(2.4 \pm 1.2) \times 10^{-2}$ | solid NaCl | 296 | 22 | |
| $\gamma_{ch}$ | $\gamma_{ch}^{-1} = a_{ch} + b_{ch}[ClONO_2]$; $a_{ch} = 74.7 \pm 7.7(1\sigma)$; $b_{ch} = (1.9 \pm 0.1(1\sigma)) \times 10^{-11}$ molecules$^{-1}$cm$^3$ | polycrystalline film | 293 | this work | $[ClONO_2] = (0.5-25) \times 10^{12}$ molecules cm$^{-3}$; a mechanism of initial and steady-state uptake is proposed; a number of elementary rate constants are determined |
| $\gamma_s$ | $\gamma_s^{-1} = a_s + b_s[ClONO_2]$; $a_s = 521 \pm 61(1\sigma)$; $b_s = (14.8 \pm 0.6(1\sigma)) \times 10^{-11}$ molecules$^{-1}$cm$^3$ | polycrystalline film | 293 | this work | |
| $\gamma_s$ | $(6.0 \pm 0.9(1\sigma)) \times 10^{-3}$ | polycrystalline film | 387 | this work | $\gamma_s$ values are described at 293 and 387 K in the framework of the common kinetic model |

rewrite eq 27 in the form

$$\gamma_s^{-1} = a_s + b_s\, n_V \tag{28}$$

where

$$a_s = \frac{1}{\alpha\, f_{ph}}\left(1 + \frac{k_d}{k_r}\right) \quad b_s = \frac{1}{f_{ph}}\frac{c}{4k_r Z_0}, \quad n_{th} = \frac{a_s}{b_s} \tag{29}$$

The parameters $a_s = 521 \pm 62(1\sigma)$ and $b_s = (14.8 \pm 0.55(1\sigma)) \times 10^{-11}$ molecules$^{-1}$ cm$^3$ were determined from linear regression of the data in Figure 8 by eq 28. The ratio $a_s/b_s$ gives the threshold volume concentration $n_{th} = (3.5 \pm 0.4) \times 10^{12}$ molecules cm$^{-3}$ at $T = 293$ K. The rate constants $k_r = 0.3 \pm 0.2$ s$^{-1}$ and $k_d = 34.7 \pm 4.3$ s$^{-1}$ are evaluated from eq 29 at $\alpha = 1$ and $f_{ph} = 0.2$. The value of $f_{ph}$ follows from the model assumption $[Z_{ch}(t)] + [Z_{ph}(t)] = f\, Z_0^{NaCl}$, where $f = 0.2$ and $[Z_{ch}(t \rightarrow \infty)] = 0$. Note that $\gamma_s$ has a maximum value at $[ClONO_2] \ll n_{th}$, that is, at low population of the surface by adsorbed molecules

$$\gamma_s^{(max)} \cong \alpha\, f_{ph}(k_r/k_d) = 1/a_s \tag{30}$$

Taking into account Arrhenius expressions for $k_r = A_r \exp(-E_r/RT)$ and $k_d = A_d \exp(-Q/RT)$, the $\gamma_s^{(max)}$ will increase if $E_r > Q$ when temperature rises. Otherwise, for $E_r < Q$, the $\gamma_s^{(max)}$ will decrease. Here $A_r$ and $A_d$ are preexponential factors independent of temperature, $E_r$ is activation energy of unimolecular decomposition, and $Q$ is the heat of adsorption. It follows from Figure 8 that the inequality $E_r > Q$ is realized. The ratio of $\gamma_s$ (387 K) $= (6 \pm 0.9(1\sigma)) \times 10^{-3}$ to $\gamma_s^{max}$(293 K) $= (1.9 \pm 0.1(1\sigma)) \times 10^{-3}$ gives

$$E_r - Q = (11.5 \pm 1.6)\ \text{kJ mole}^{-1} \tag{31}$$

The value of $Q = (64.3 \pm 0.3)$ kJ mole$^{-1}$ follows from $k_d$ (293 K) $= (34.7 \pm 4.3)$ s$^{-1}$, supposing a normal preexponential factor $A_d \cong 10^{13}$ s$^{-1}$. The sum of eq 31 and calculated $Q$ gives the activation energy $E_r = (75.8 \pm 1.6)$ kJ mole$^{-1}$.

The threshold volume concentration $n_{th}$(387 K) can be evaluated by eq 29, taking into account the Arrhenius expressions for $k_r$ and $k_d$. This value is found to be $1.8 \times 10^{15}$ molecules cm$^{-3}$ for $\alpha = 1$. Thus, $n_{th}$(387 K) $\gg [ClONO_2]$ in the range of $ClONO_2$ volume concentrations exploited. In this case, the $\gamma_s$ is expressed by eq 30 and must be independent of $[ClONO_2]$.

Table 1 summarizes all of the elementary constants found that characterize the initial and steady-state steps of the uptake. The indicated uncertainties correspond to one standard error. The values of $n_{th}$ and $k_d$ are seen to be identical, whereas the rate constants of unimolecular decomposition differ by 1 order of magnitude. This means that the difference between the surface complexes $ClONO_2 \cdots Z_{ch}$ and $ClONO_2 \cdots Z_{ph}$ is likely to be determined by their different reactivity rather than by their adsorption/ desorption properties.

**Comparison with Literature Results.** Shown in Table 2, the uptake coefficients determined in reviewed studies are dramatically different in value. The partial uptake coefficients leading to a formation of the prime gas-phase products were not measured. Further, initial and steady-state steps of the uptake were not defined in details.

Generally, $\gamma_{ch}$ and $\gamma_s$ turn out to be dependent on $ClONO_2$ concentration. This enables us to identify elementary stages of the uptake process and to evaluate parameters of the two uptake stages. The final objective of our approach is to extrapolate laboratory data to real troposphere conditions. The value of $\gamma \cong 0.1$ is proposed by Rossi[34] to be a consistent value. Our $\gamma_{ch}$ and $\gamma_s$ for "dry" salt at $T = 293$ K are much lower compared to his value. Maximum values of $\gamma_{ch}$ and $\gamma_s$ are observed at low $[ClONO_2]$, that is, $\gamma_{ch}$ ($[ClONO_2] \rightarrow 0$) $\cong 10^{-2}$ and $\gamma_s$ ($[ClONO_2] \rightarrow 0$) $\cong 2 \times 10^{-3}$. These values are closest to those of Timonen et al.,[17] $\gamma_s = (4.6 \pm 3.1) \times 10^{-3}$, and Hoffman et al.,[22] $\gamma_{0,s} = (2.4 \pm 1.2) \times 10^{-2}$. These lower values are unlikely to explain high concentration of $Cl_2$ observed in the MBL regions by some field measurements.[9] However, according to our preliminary data, $\gamma$ increases in direct proportion to the relative humidity (RH). It can reach value of ~0.1 at RH of 20−30%, when NaCl particles will still be solid. At such a high uptake coefficient, self-catalyzed extraction of $Cl_2$ from NaCl is possible in MBL regions polluted with nitric oxides.[13−15] All of these points deserve to be weighed carefully. In the next paper, the dependence of the $ClONO_2$ uptake on humidified NaCl will be considered and discussed.

**Acknowledgment.** Yu.M.G. thanks Prof. B. J. Finlayson-Pitts and her colleagues for interesting and useful discussions during his visit to University of California, Irvine. Also, Yu.M.G. and V.V.Z. thank all of the participants of the NSF project "Atmospheric Integrated Research for Understanding Chemistry of Interface (AIR UCI)" for active and useful discussion on results of this paper during the 1st Workshop of Environmental Molecular Science Institutes (June 25−30, 2005). We understand that this work would be impossible without the support of U.S. CRDF (award RC2-2521-MO-03) and RFBR (grants 00-03-32999 and 03-03-32711).

## References and Notes

(1) Farman, J. C.; Gardiner, B. C.; Shanklin, J. D. *Nature* **1985**, *315*, 207.
(2) Molina, M. J.; Rowland, F. S. *Nature* **1974**, *249*, 810.
(3) Bottenheim, J. W.; Galant, A. C.; Brice, K. A. *Geophys. Res. Lett.* **1986**, *13*, 113.
(4) Oltmans, S. J.; Komhyr, W. D. *J. Geophys. Res.* **1986**, *91*, 5229.
(5) Platt, U. *Water, Air, Soil Pollut.* **2000**, *123*, 229.
(6) Sander, R.; Crutzen, P. J. *J. Geophys. Res. D* **1996**, *101*, 9121.
(7) Wang, T. X.; Margerum, D. W. *Inorg. Chem.* **1994**, *33*, 1050.
(8) Beckwith, R. C.; Wang, T. X.; Margerum, D. W. *Inorg. Chem.* **1996**, *35*, 995.
(9) Spicer, C. W.; Chapman, E. G.; Finlayson-Pitts, B. J.; Plastridge, R. A.; Hubbe, J. M.; Fast, J. D.; Berkowitz, C. M. *Nature* **1998**, *394*, 353.
(10) Foste, K. L.; Plastridge, R. A.; Bottenheim, J. W.; Shepson, B.; Finlayson-Pitts, B. J.; Spicer, C. W. *Science* **2001**, *291*, 471.
(11) Singh, H. B.; Gregory, G. L.; Anderson, B.; Browell, E.; Sachse, G. W.; Davis, D. D.; Crawford, J.; Bradshaw, J. D.; Talbot, R.; Blake, D. R.; Thornton, D.; Newell, R.; Merrill, J. *J. Geophys. Res.* **1996**, *101*, 1907.
(12) Pszenny, A. A. P.; Keene, W. C.; Jacob, D. J.; Fran, S.; Maben, J. R.; Zetwo, M. P.; Sringer-Young, M.; Galloway, J. N. *Geophys. Res. Lett.* **1993**, *20*, 699.
(13) Gershenzon, M. Yu.; Grigorieva, V. M.; Il'in, S. D.; Remorov, R. G.; Shestakov, D. V.; Zelenov, V. V.; Aparina, E. V.; Gershenzon, Yu. M. Global Atmospheric Change and Its Impact on Regional Air Quality. *Nato Science Series. IV. Earth and Environmental Science*; Barnes, I., Ed.; Kluwer Academic Publishers: Boston, MA, 2002; Vol. 16, p 109.
(14) Gershenzon, M. Yu.; Grigorieva, V. M.; Shestakov, D. V.; Zelenov, V. V.; Gershenzon, Yu. M.; Zellner, R. The Mechanism of Heterogeneous "Self-Cleaning" of the Coastal Troposphere. May it Have an "Explosion-like" Autocatalytic Character? *Combustion and Atmospheric Pollution*; Roy, G. D., Ed.; Frolov, S. M.; Starik, A. M. Torus-Press: Moscow, 2003; p 390.
(15) Gershenzon, M. Yu.; Grigorieva, V. M.; Il'in, S. D.; Shestakov, D. V.; Gershenzon, Yu. M.; Zellner, R.; Finlayson-Pitts, B. J. Mechanism of "Chlorine Explosion" in the $NO_x$-Enriched Troposphere. *Combustion and Pollution: Atmospheric Impact*; Roy, G. D., Ed.; Frolov, S. M.; Starik, A. M. Torus-Press: Moscow, 2005; p 117.
(16) Finlayson-Pitts, B. J.; Ezell, M. J.; Pitts, J. N. *Nature* **1989**, *337*, 241.

(17) Timonen, R. S.; Chu, L. T.; Leu, M.-T.; Keyser, L. F. *J. Phys. Chem*. **1994**, *98*, 9509.
(18) Caloz, F.; Fenter, F. F.; Rossi, M. J. *J. Phys. Chem.* **1996**, *100*, 7494.
(19) Koch, T. G.; Rossi, M. J. *J. Phys. Chem. A* **1998**, *102*, 9193.
(20) Aguzzi, A.; Rossi, M. J. *Phys. Chem. Chem. Phys.* **1999**, *1*, 4337.
(21) Gebel, M.; Finlayson-Pitts, B. J. *J. Phys. Chem. A.* **2001**, *105*, 5178.
(22) Hoffman, R. C.; Gebel, M. E.; Fox, B. S.; Finlayson-Pitts, B. J. *Phys. Chem. Chem. Phys*. **2003**, *5*, 1780.
(23) Zelenov, V. V.; Loboda, A. V.; Aparina, E. V.; Dodonov, A. F. *Izvestia RAS, Energ*. **1997**, *1*, 70.
(24) Brauer, G. *Handbook on Inorganic Synthesis*; MIR: Moscow, 1985.
(25) Gershenzon, Yu. M.; Grigorieva, V. M.; Zasypkin, A. Yu.; Remorov, R. G. Kinetic resistance additivity for coaxial reactor. 13th Int. Symp. on Gas Kinetics, Dublin, Ireland, Sept. 11−16, 1994. *Book of Abstracts*, p 420.
(26) Gershenzon, Yu. M.; Grigorieva, V. M.; Ivanov, A. V.; Remorov, R. G. *Faraday Discuss*. **1995**, *100*, 83.
(27) Franck-Kamenetskii, D. A. *Diffusion and Heat Change in Chemical Kinetics*: Nauka, Moscow, 1967.
(28) Schack, C. J. *Inorg. Chem*. **1967**, *6*, 1938.
(29) Zelenov, V. V.; Aparina, E. V.; Shestakov, D. V.; Gershenzon, Yu. M. *Khim. Fiz.* **2004**, *23*, 18.
(30) Gershenzon, M. Yu.; Il'in, S. D.; Fedotov, N. G.; Gershenzon, Yu. M.; Aparina, E. V.; Zelenov, V. V. *J. Atmos. Chem.* **1999**, *34*, 119.
(31) Zelenov, V. V.; Aparina, E. V.; Gershenzon, M. Yu.; Il'in, S. D.; Gershenzon, Yu. M. *Khim. Fiz.* **2002**, *21*, 42.
(32) Zelenov, V. V.; Aparina, E. V.; Gershenzon, M. Yu.; Il'in, S. D.; Gershenzon, Yu. M. *Khim. Fiz.* **2003**, *22*, 37.
(33) Zelenov, V. V.; Aparina, E. V.; Gershenzon, M. Yu.; Il'in, S. D.; Gershenzon, Yu. M. *Khim. Fiz.* **2003**, *22*, 59.
(34) Rossi, M. J. *Chem. Rev.* **2003**, *103*, 4605.
(35) Dementiev, A. P.; Zelenov, V. V.; Aparina, E. V.; Shestakov, D. V.; Il'in, S. D.; Gershenzon, Yu. M. *Khim. Fiz.* **2004**, *23*, 54.
(36) Dai, D. J.; Peters, S. J.; Ewing, G. E. *J. Phys. Chem*. **1995**, *99*, 10299.
(37) Kittel, C. *Introduction to Solid State Physics*, 6th Ed.; Wiley: New York, 1986.
(38) Dai, D. J.; Ewing, G. E. *J. Phys. Chem*. **1993**, *98*, 5050.
(39) Finlayson-Pitts, B. J. *Chem. Rev*. **2003**, *103*, 4801.
(40) Seisel, S.; Fluckiger, B.; Caloz, F.; Rossi, M. J. *Phys. Chem. Chem. Phys*. **1999**, *1*, 2257.